A nonmineralized approach to abrasion-resistant biomaterials

Michael G. Pontin*, Dana N. Moses†, J. Herbert Waite†, and Frank W. Zok*‡

*Materials Department and †Marine Science Institute, University of California, Santa Barbara, CA 93106-5050

Edited by John W. Hutchinson, Harvard University, Cambridge, MA, and approved June 22, 2007 (received for review March 12, 2007)

The tooth-like mouthparts of some animals consist of biomacromolecular scaffolds with few mineral components, making them intriguing paradigms of biostructural materials. In this study, the abrasion resistance of the jaws of one such animal, the bloodworm *Glycera dibranchiata*, has been evaluated by nanoindentation, nanoscratching, and wear testing. The hardest, stiffest, and most abrasion-resistant materials are found within a thin (<3 μm) surface layer near the jaw tip and a thicker (10–20 μm) subsurface layer, both rich in unmineralized Cu. These results are consistent with the supposition that Cu ions are involved in the formation of intermolecular coordination complexes between proteins, creating a highly cross-linked molecular network. The intervening layer contains aligned atacamite [$Cu_2(OH)_3Cl$] fibers and exhibits hardness and stiffness (transverse to the alignment direction) that are only slightly higher than those of the bulk material but lower than those of the two Cu-rich layers. Furthermore, the atacamite-containing layer is the least abrasion-resistant, by a factor of ≈3, even relative to the bulk material. These observations are broadly consistent with the behavior of engineering polymer composites with hard fiber or particulate reinforcements. The alignment of fibers parallel to the jaw surface, and the fiber proximity to the surface, are both suggestive of a natural adaptation to enhance bending stiffness and strength rather than to endow the surface regions with enhanced abrasion resistance.

glycera jaw | nanoindentation | scratching | wear

Most animals possess dentitions that are well adapted to a variety of piercing, biting, and grinding functions. Mammalian teeth, for example, are highly mineralized tissues consisting of a dentin core (>70% mineral) surrounded by an outer enamel layer (>90% mineral). Mineral components are thought to be indispensable for the observed hardness, stiffness, and abrasion resistance of both portions (1). In stark contrast, the tooth-like mouthparts of many lesser-known animals, including squids, insects, spiders, and polychaete worms, consist of biomacromolecular scaffolds with little or no mineral components (2, 3). The success of these creatures begs the question as to whether mineralization is essential for effective dentition. The present study deals with one such moderately mineralized mouthpart: the jaw of the worm *Glycera dibranchiata*.

Glycera is a marine polychaete worm with four eversible jaws (Fig. 1) (4–7). The jaws consist mainly of proteins (43%) and melanin (39%) (8). Previous studies suggest that melanin forms the structural framework of the jaws, perhaps providing a scaffold onto which the other components are assembled (9). The jaws also contain small amounts of Cu and Cl (5–10%), which combine to form atacamite [$Cu_2(OH)_3Cl$] fibers (7). The fibers are found mainly in the near-tip regions of the jaw, as well as in those surrounding the venom canal. One inference is that the fibers act as reinforcements to enhance strength, as well as impact and wear resistance, in the most heavily stressed regions of the jaw. Some Cu is also present in nonmineralized form, mainly in near-surface regions, and may act to harden and stiffen the jaw by forming cross-links between the melanin and the jaw proteins.

Current understanding of the mechanical properties of *Glycera* jaws has been derived principally from depth-sensing nanoindentation (7, 9). In a typical series of measurements, 200 indentations, each ≈1 μm in size, are laid down in a periodic array with a spacing of 10 μm. The Cu and Cl distributions of the tested region are subsequently mapped by using either energy dispersive spectroscopy (EDS) or electron probe microscopy. Thus far, the resolution of the measurements has been limited by the indentation separation distance: selected to be sufficiently large in relation to the indentation size to mitigate interactions between neighboring plastic zones.

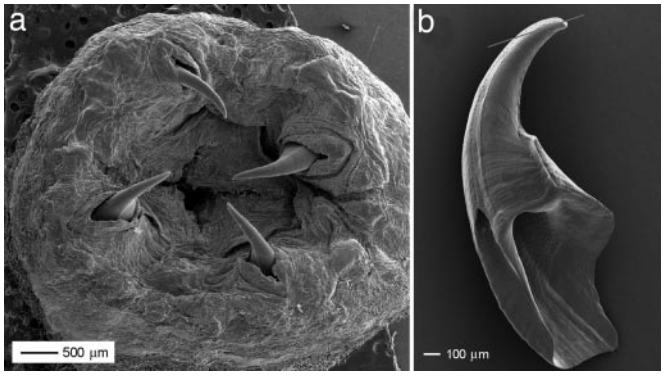

Fig. 1. SEM micrographs of a *Glycera* proboscis, showing the four eversible jaws (*a*) and a single extracted jaw (*b*). Line in *b* indicates the approximate orientation of microtomed sections.

The aim of the present study was to further elucidate the connections between composition and properties through the use of higher resolution measurement methods. The first was nonperiodic nanoindentation, in which the individual indents were more closely and accurately placed to identify mechanical property changes over shorter length scales. The second method involved scratching, using indenters similar to those used for nanoindentation. Because of the continuous nature of these measurements, property gradients and discontinuities across interphase boundaries can be more readily identified. Additional insights into abrasion resistance were gleaned through wear tests. These were performed by repeatedly rastering the indenter over a prescribed area with a constant normal force and subsequently mapping changes in surface topography. The mechanical measurements were accompanied by microstructural examinations and compositional analyses using a combination of scanning probe microscopy (SPM), EDS,

Author contributions: M.G.P. and D.N.M. contributed equally to this work; M.G.P., D.N.M., J.H.W., and F.W.Z. designed research; M.G.P. and D.N.M. performed research; M.G.P., D.N.M., and F.W.Z. analyzed data; and J.H.W. and F.W.Z. wrote the paper.

The authors declare no conflict of interest.

This article is a PNAS Direct Submission.

Abbreviations: EDS, energy dispersive spectroscopy; SPM, scanning probe microscopy; BEI, backscatter electron images.

‡To whom correspondence should be addressed. E-mail: zok@engineering.ucsb.edu.

This article contains supporting information online at www.pnas.org/cgi/content/full/0702034104/DC1.

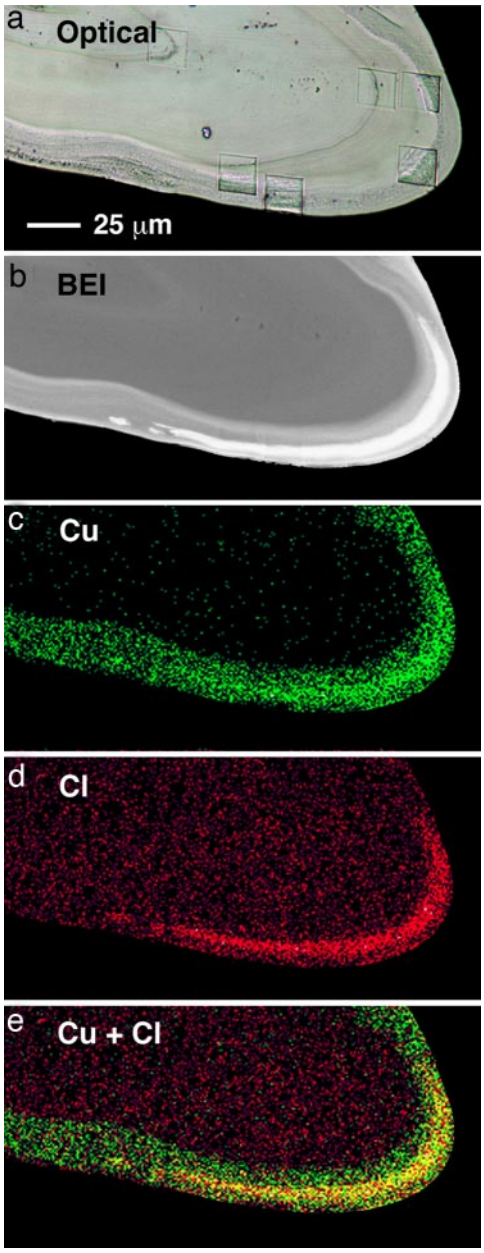

Fig. 2. Optical and backscatter electron (BEI) images of the near-tip region of a microtomed *Glycera* jaw along with corresponding Cu and Cl distributions, obtained by EDS. Superposition of the Cu and Cl distributions (in *e*) reveals the atacamite-containing regions (shown in yellow). Square features in *a* are a remnant of wear tests.

and optical microscopy, as well as scanning electron microscopy (SEM) and transmission electron microscopy (TEM). Taken together, these measurements and observations yield insights into the nature of the microstructure in the near-surface region of the jaws and the graded nature of their properties. Interestingly, our findings suggest that the mineralized portions of the jaw tip are not the most abrasion resistant.

Results and Analysis

Microstructure. The microscopic examinations revealed four distinct microstructural domains in the near-surface region of the jaw tip (Fig. 2):

1. A thin (0.5–3 μm) layer, denoted A, exists along the outer jaw surface. The microtomed surface in this region appears smooth in both optical micrographs and SPM images. Copper is present in significant amounts and thus this region appears bright in backscatter electron images (BEI). The absence of Cl or other inorganic elements indicates that the Cu exists in nonmineralized form.
2. Moving toward the jaw interior, the second layer, denoted B, is rougher than the first and is typically 5–15 μm thick. Both Cu and Cl are present in significant quantities, consistent with the presence of atacamite fibers (shown below). BEI of this layer appears the brightest. The surface roughness is attributable to differences in mechanical properties and hence cutting characteristics of the atacamite fibers and the surrounding organic matrix. SPM images (presented later) reaffirm this conclusion.
3. The third layer, denoted C, is similar to region A in almost all respects. It is smooth, contains nonmineralized Cu (without Cl) and exhibits similar brightness levels in BEI. The only apparent difference is its thickness, which is typically 10–20 μm.
4. The bulk of the jaw (D) is also smooth but contains no detectable levels of Cu, Cl, or other notable elements. Consequently, it appears darkest in BEI mode.

The presence of atacamite fibers in region B was confirmed by TEM (Fig. 3). The fibers appear darker than the surrounding matrix due to the presence of heavy elements, notably Cu and Cl. They are ≈50–70 nm in diameter, consistent with previous measurements (7), and aligned approximately parallel to the external jaw surface.

Indentation. Hardness and modulus profiles across the four microstructural domains are plotted in Fig. 4. The locations of the domain boundaries were inferred from the spatial variations in properties and confirmed by SPM imaging. The nonmineralized Cu-rich regions (A and C) exhibited the highest hardness and stiffness ($H \approx 0.8$ GPa, $E \approx 10$ GPa) and were virtually indistinguishable from one another. The properties of the bulk (D) and the atacamite-containing material (B) were clearly below those of A and C. Additionally, the properties of B were only slightly higher than those of D, indicating that the atacamite fibers play only a minor role. The bulk properties ($H \approx 0.7$ GPa, $E \approx 9$ GPa) were comparable to those reported in previous studies (7, 9).

Although the peak hardness and modulus values obtained in the present study also agree with those reported previously, the correlations between these properties and the microstructure differ significantly. Previous examinations of similar regions of *Glycera* jaws had successfully identified the presence of the atacamite-containing layer in the near-surface region, but not the adjacent nonmineralized Cu-rich region. With the highest hardness and modulus also being obtained in approximately the same region, the property elevations had been attributed principally to the presence of the mineral phase (7), a problem previously noted (10). In contrast, the present results clearly show that the peak mechanical properties are obtained in regions rich in nonmineralized Cu, not in those containing atacamite fibers. Corroborating evidence has been obtained from the scratch tests, which are presented below.

Scratch Resistance. Representative measurements from scratch tests are plotted in Figs. 5–8. Material response was characterized by two parameters: the normalized friction force, F_L/F_N (F_N and F_L being the normal and lateral forces, respectively) and the scratch depth, u_N. Three key features emerge.

1. The normal penetration depth during scratching reached a steady state after ≈1 μm of lateral displacement and was only slightly greater (5–10%) than that obtained following application of the normal force (Fig. 5). The implication is that the scratch depth is dominated by material hardness.
2. The penetration depths both upon initial normal loading and during scratching were greatest in the atacamite-containing material (B) and the bulk (D) for all load levels. Moreover, the

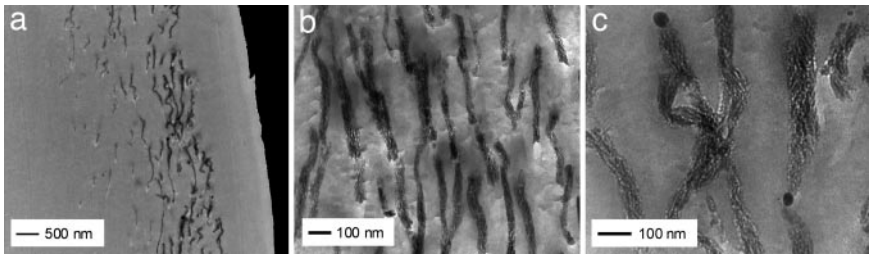

Fig. 3. TEM images at progressively increasing magnifications, revealing layers of atacamite fibers oriented parallel to the jaw surface as well as a distinct (≈1 μm) atacamite-free zone near the surface.

depths in A and C were similar to one another and lower than those in B and D (Fig. 6). These trends are consistent with the nanoindentation measurements.

3. The normalized scratch force, F_L/F_N, in B was greatest in magnitude and exhibited the greatest fluctuations with indenter position: the latter attributable to the inherently heterogeneous nature of the atacamite-containing material. The scratch forces in D were only slightly lower, whereas those in A and C were consistently lowest.

Additional confirmation of the preceding trends were obtained from studies on the effects of F_N on F_L/F_N, coupled with a mechanics model of plowing of a perfectly plastic material by a hard spherical indenter [see supporting information (SI) *Text*]. The model predicts that the scratch force can be partitioned into two components: one governed by frictional sliding, in accordance with Coulomb's law, and the other associated with plastic deformation. The predicted scratch force is given by

$$\frac{F_L}{F_N} = \mu + \beta\sqrt{\frac{F_N}{R^2H}}, \qquad [1]$$

where μ is the friction coefficient (that is, the force ratio F_L/F_N for a purely elastic contact); R is the indenter radius of curvature; and β is a nondimensional coefficient of order 1/20.

Accordingly, the experimental results in Figs. 5 and 6 as well those from many additional tests have been compiled and presented as F_L/F_N vs. $\sqrt{F_N}$ (Fig. 8*b*). In this form, the results for each microstructural domain are linear (correlation coefficients, $r^2 > 0.9$), as suggested by Eq. **1**. The inferred friction coefficients for all domains, obtained by extrapolating the data to F_N, were similar to that measured directly by using a 50 μm radius indenter ($\mu = 0.23 \pm 0.02$), wherein the contact is purely elastic (Fig. 8*a*). (Detailed analysis indicates that the inferred friction coefficients in the four domains fall in the range 0.21–0.25 and that their differences are not statistically significant.) Recognizing that the slopes of the lines in Fig. 8*b* scale with $1/\sqrt{H}$, the material in B emerges as the softest, and those in C and A the hardest. These results reaffirm the earlier hardness rankings.

Wear. Representative results from the wear tests are summarized in Fig. 9. From the SPM images as well as the Cu and Cl EDS maps, the boundaries between the four microstructural domains have been ascertained and are indicated on the figures by the dotted lines. The wear depth map (Fig. 9*c*) revealed that the atacamite containing region exhibited the highest wear rate, by a factor of ≈3 relative to that of adjacent layers. These differences were further illustrated by typical line scans through each of the four domains, plotted in Fig. 10. Several other wear tests performed on similar regions of the jaw cross-section yielded the

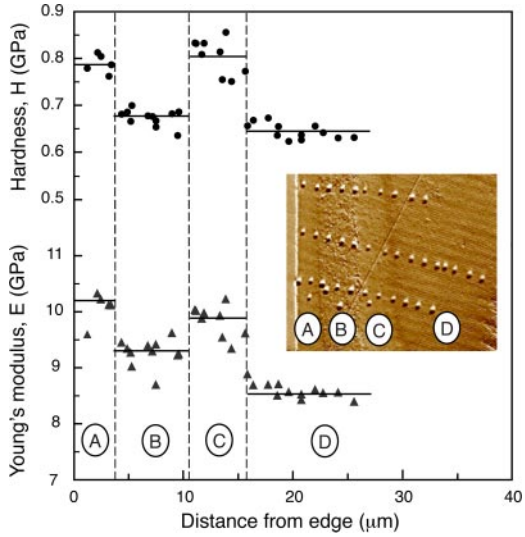

Fig. 4. Hardness and modulus profiles across the four microstructural domains of the jaw cross-section. (*Inset*) An SPM image showing the layers and a typical indent pattern.

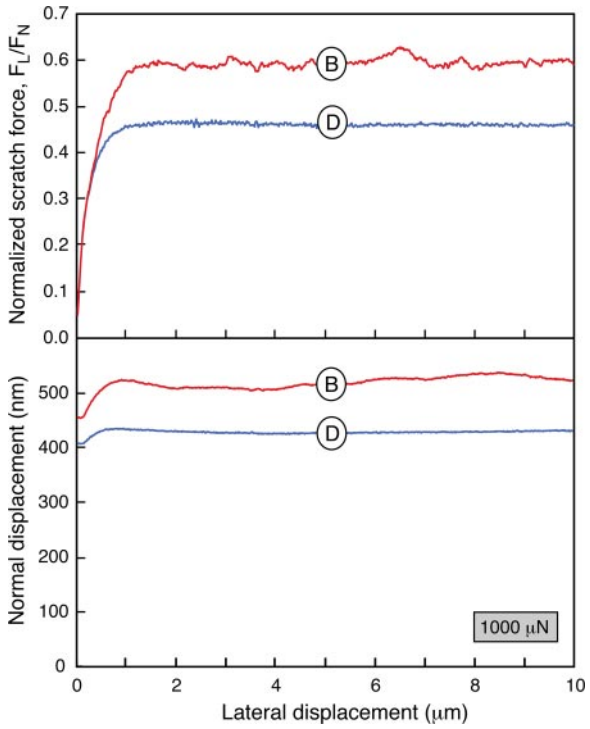

Fig. 5. Representative scratch measurements made within regions B and D (not across interfaces).

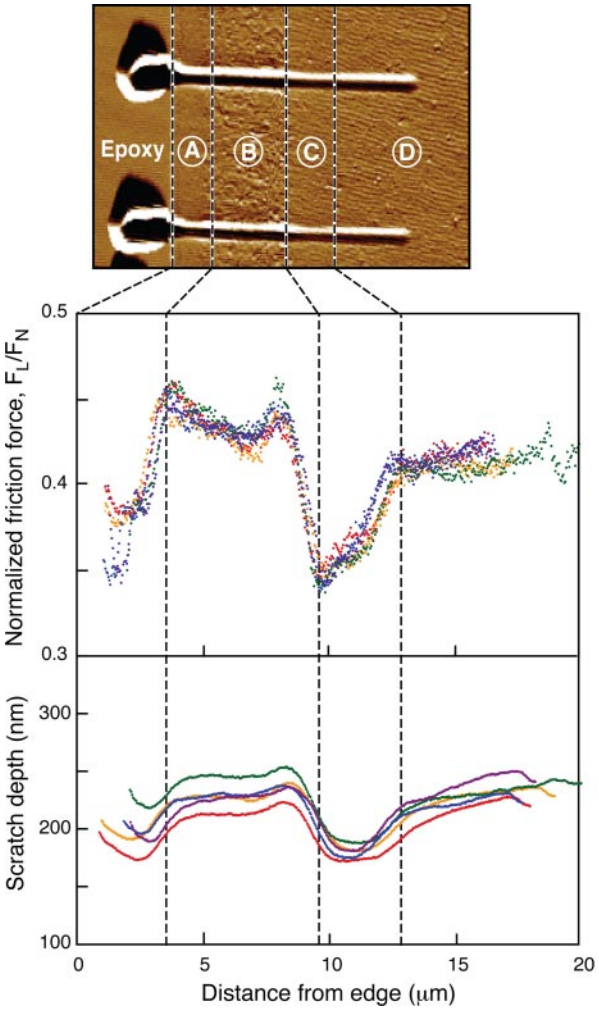

Fig. 6. Representative scratch measurements made within regions A, B, C, and D (across layers). Each curve is from an individual scratch (F_N = 500 μN). Note the change in both the scratch force and the scratch depth at the C/D interface, despite the absence of any obvious difference in surface appearances in the SPM image (*Upper*).

same trends in wear resistance. Namely, region B always exhibited the highest degree of wear.

Discussion

The present experimental investigation has revealed the presence of four distinct microstructural domains in the near-tip regions of the *Glycera* jaw. The results differ from those reported earlier in at least one important respect: the highest hardness and modulus are obtained within the two nonmineralized Cu-rich regions, not in the region containing atacamite fibers. Previous assertions that the atacamite fibers are largely responsible for the high local hardness and modulus were likely due to the failure to clearly delineate the mineralized and nonmineralized regions. Indeed, the nonmineralized Cu-rich region was somewhat fortuitously identified in the present study from the scratch tests. That is, in traversing from the interior to the exterior (right to left in Fig. 6), distinct and reproducible changes in scratch force and scratch depth were obtained at the C/D interface, despite the absence of obvious changes in surface topography (see, for example, top image in Fig. 6). These initially puzzling results prompted the subsequent optical and SEM examinations as well as EDS measurements.

The rather unimpressive hardness and modulus of the atacamite-containing material stem largely from the fact that the indentation

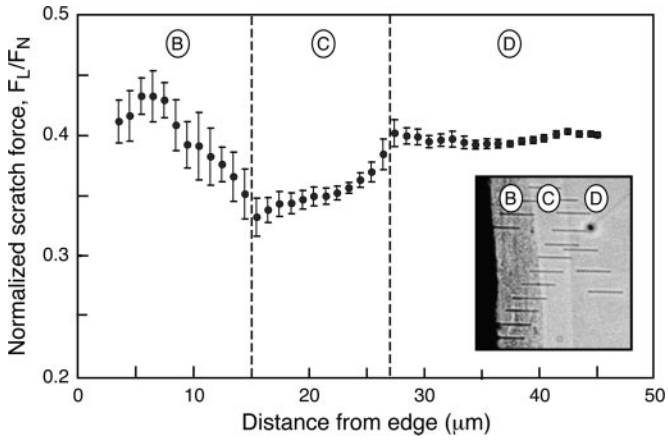

Fig. 7. Average scratch forces for tests performed across layers B, C, and D (F_N = 500 μN). Each datum point represents the mean of ≈150 measurements, and the error bars are one standard deviation from the mean.

and scratch measurements were performed essentially perpendicular to the direction of fiber alignment. Treating this material as a unidirectionally reinforced fiber composite, its transverse Young's modulus E_T can be estimated from the Reuss lower bound, notably

$$E_T = (f/E_f + (1 - f)/E_m)^{-1}, \quad [2]$$

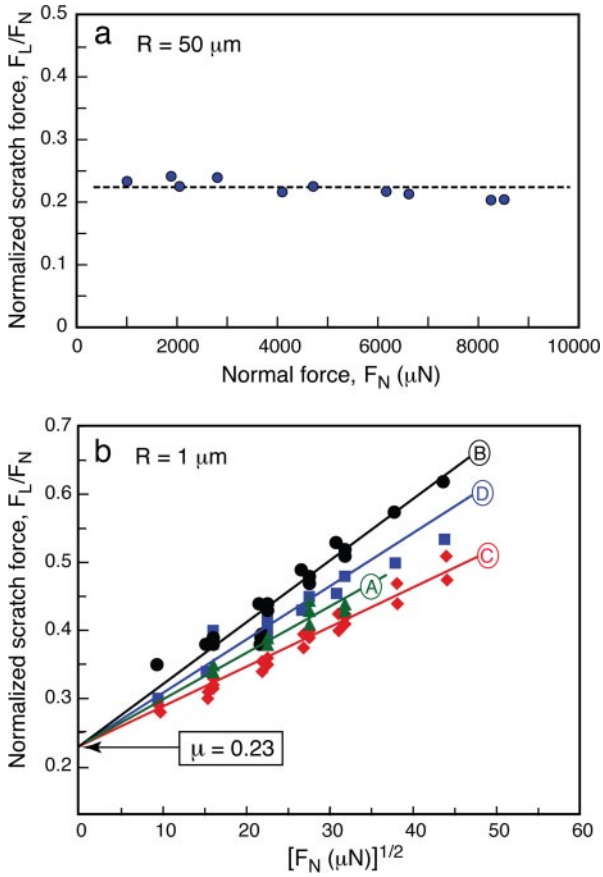

Fig. 8. Effects of normal force on the normalized scratch force, for indenter tip radii of 50 μm (*a*) and 1 μm (*b*). In *a*, the contact is purely elastic, as manifested in complete and immediate recovery of normal displacement after unloading. The resulting normalized scratch force is independent of normal force and represents the friction coefficient.

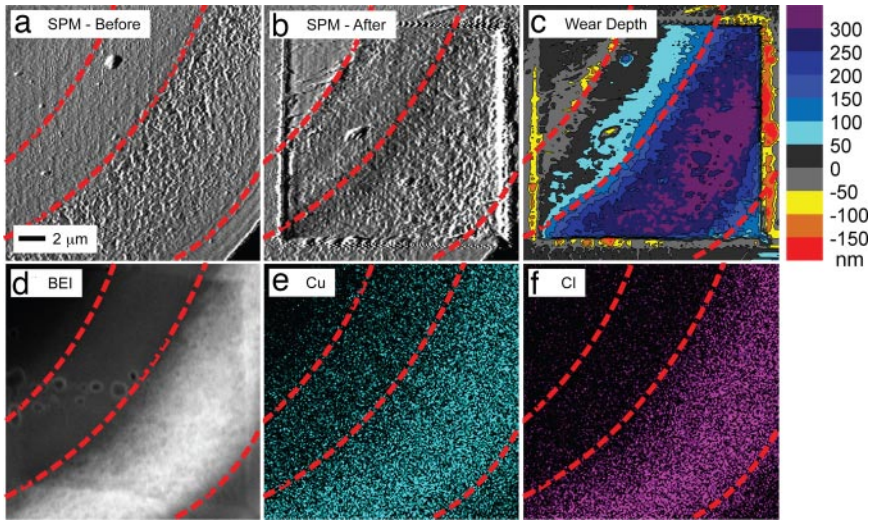

Fig. 9. Summary of results from a representative wear test performed on a near-surface region that encompasses the four microstructural domains.

where f is the fiber volume fraction and E_f and E_m are the fiber and matrix modulus, respectively. For $f = 0.15$ and $E_f/E_m = 5$ (values approximately representative of the atacamite-containing material), the predicted modulus ratio is $E_T/E_m \approx 1.14$: broadly consistent with the measurements shown in Fig. 4. The corresponding change in the transverse yield strength and hence hardness are predicted to be even lower. Numerical simulations using finite element methods have shown that the elevations in yield strength over the matrix values are negligible in the volume fraction domain of interest. For instance, for $f = 0.15$, the composite to matrix strength ratio σ_T/σ_m ranges from 1.00 for square fiber arrays to 1.03 for hexagonal arrays (11). These predictions are in accord with the small differences in the hardnesses of regions B and D in Fig. 4.

The poor abrasion resistance of the atacamite-containing material, especially in relation to the surrounding nonmineralized Cu-rich material, is broadly consistent with the results of macroscopic wear tests on engineering fiber composites. For instance, additions of mineral fillers (12) or hard continuous fibers (13–15) (aramid, carbon, or glass) to polymer matrices invariably increase wear rates, by as much as a factor of 10. These observations suggest that the outermost jaw layer, although very thin, plays a crucial role in protecting the underlying atacamite fibers from abrasion by sand grains and the prey carapace. They also lead to speculation on nature's motive for placing the atacamite fibers in the near-surface, near-tip regions of the *Glycera* jaws. One possibility is that the fibers impart high bending stiffness and strength in the most highly stressed regions of the jaw. Indeed, the alignment of fibers parallel to the jaw surface as well as their proximity to the free surface are consistent with established design principles for engineering structures that support bending loads (16). That is, the most efficient use of fibers is achieved by aligning them parallel to the principal stress directions and placing them at the greatest distance from the axis of bending. The stiffness enhancement associated with the fibers subject to loading parallel to the alignment direction can be estimated from the Voigt average

$$E_L = fE_f + (1 - f)E_m. \quad [3]$$

Taking $f = 0.15$ and $E_f/E_m = 5$ (as before) yields a modulus ratio $E_L/E_m \approx 1.60$. Further assuming that the fibers are at least as strong as the matrix, the longitudinal composite strength is bounded by $\sigma_T/\sigma_m \geq E_L/E_m \approx 1.60$. Clearly, the benefit of the fibers to bending resistance would be considerably greater than that to abrasion resistance.

Perhaps of greatest significance to our understanding of the design of bioengineering materials is the elevation in hardness and stiffness associated with nonmineralized Cu. The role of Cu as well as other metal ions in mechanical properties of bioorganic materials has been speculated to involve formation of intermolecular coordination complexes, creating a highly cross-linked molecular network. Although this effect has been clearly demonstrated in the case of Zn ions in the jaws of *Nereis* worms (17), it has been less compelling in the *Glycera* jaws because of the presence of Cu-containing atacamite fibers in neighboring regions. The present study indicates that Cu ions do indeed play a significant role in the mechanical properties of *Glycera* jaws, elevating the hardness and stiffness to levels that are about twice those obtained in the very best engineering polymers.

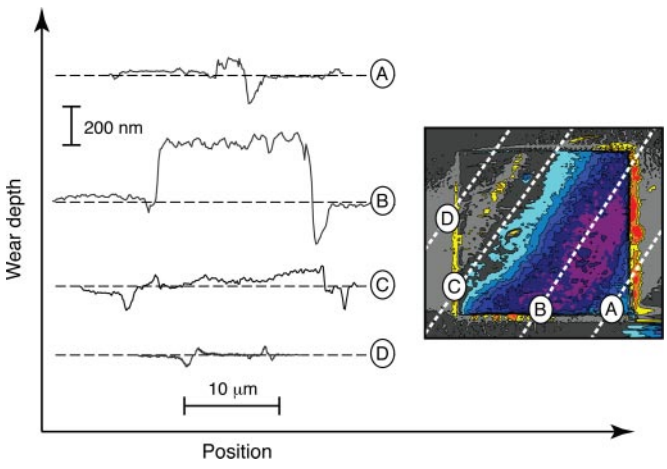

Fig. 10. Wear depth profiles within each of the four microstructural domains.

Conclusions

The use of scratch testing has proven to be a valuable tool in both elucidating the variations in mechanical properties and identifying the pertinent microstructural domains in the near-tip regions of the *Glycera* jaw. Wear testing has yielded complementary information on the robustness of the various domains and provided further clues on their intended roles. Although the role of the atacamite fibers remains to be definitively elucidated,

the relatively low hardness, modulus and abrasion resistance of the atacamite-containing regions subject to loading perpendicular to the direction of fiber alignment suggests that their predominant role is not one of enhancing abrasion resistance. Instead, they likely serve as reinforcements against the macroscopic bending loads that arise during burrowing and catching prey. The thin external Cu-rich layer appears to serve the critical role of abrasion protection. The absence of Cu in the underlying bulk of the jaw may reflect nature's selective placement of chemical species that are available in only limited quantities.

Materials and Methods

Specimen Preparation and Characterization. Live *Glycera dibranchiata* worms were obtained from Maine Bait Company (Newcastle, ME). Upon delivery, the worms were frozen at −80°C, and thawed immediately before jaw extraction. The extracted jaws were immersed in water until all surrounding tissue could be readily removed with microforceps and subsequently dried in air (Fig. 1).

In preparation for microstructural characterization and mechanical testing, the jaws were embedded in epoxy molds. The jaws were oriented such that, upon sectioning, a longitudinal near-tip region was revealed on the surface, parallel to the mold surface (Fig. 1*b*). Thin (80–100 nm) sections for TEM were cut by using an ultramicrotome and transferred to copper TEM grids. The specimens were examined in a JEOL 2000FX TEM, operated at 80 kV. The bulk sample remaining in the mold was examined in an optical microscope and used for subsequent mechanical tests. After testing, the latter samples were briefly sputter-coated with gold and examined in an SEM in BEI mode. Maps of Cu and Cl distributions were also obtained in the SEM by EDS.

Mechanical Testing. Mechanical tests were conducted in ambient air using a fully automated nanomechanical test system capable of normal and lateral loading as well as *in situ* SPM (TriboIndenter; Hysitron, Minneapolis, MN). Three test types were used.

First, normal indentation tests were performed by using a 60° conical diamond indenter with a 1-μm tip radius. The maximum load during indentation was 500 μN, with loading and unloading rates of 100 μN/s, and a 60-s hold time at peak load. Hardness, H, and Young's modulus, E, were calculated from the unloading portions of the load-displacement curves following established procedures (18).

Second, scratch tests were performed by using the same indenter. The test protocol consisted of: (*i*) applying a normal load in the range 250–2,000 μN, over a time period of 5 s; (*ii*) holding at the peak load for 5 s; (*iii*) displacing the indenter tip laterally over a distance of 10–15 μm at a rate of 0.33 μm/s; and (*iv*) holding for an additional 5 s before unloading. Some scratches were fully contained within a prescribed microstructural domain whereas others traversed two or more adjacent domains. During scratching, continuous measurements were made of the normal and lateral forces, F_N and F_L, as well as the normal and lateral displacements, u_N and u_L. Complementary measurements of this type were made by using a 50 μm radius tip, over a load range 1,000–9,000 μN. In this case, the contact is purely elastic and hence F_L/F_N represents the friction coefficient, μ.

Third, wear tests were performed by rastering the indenter with a 1-μm tip radius over the surface with a prescribed load, using the SPM function of the test system. Each scan covered an area 20 × 20 μm at a rate of 120 μm/s under a normal force of 500 μN. Each test consisted of 10 scans over the prescribed area. Scan areas were selected to include the four microstructural domains. Wear depths were ascertained from low-load SPM scans, performed before and after each test. The latter scans covered an area 30 × 30 μm, encompassing the entire worn area as well as a 5-μm band of reference (pristine) material around its perimeter.

This work was supported by National Institutes of Health Bioengineering Research Partnerships Grant R01DE014672. J.H.W. and F.W.Z. are Principal Investigators for the National Institutes of Health.

1. Currey JD (1999) *J Exp Biol* 202:3285–3294.
2. Schofield RM, Nesson MH, Richardson KA (2002) *Naturwissenschaften* 89:579–583.
3. Broomell CC, Khan RK, Moses DN, Miserez A, Pontin MG, Stucky GD, Zok FW, Waite JH, (2007) *J R Soc Interface* 4:19–31.
4. Michel C, Fonze-Vignaux MT, Voss-Foucart MF (1973) *Bull Biol Fr Belg* 107:301–321.
5. Voss-Foucart MF, Fonze-Vignaux MT, Jeuniaux C (1973) *Biochem Syst* 1:119–122.
6. Gibbs PE, Bryan GW (1980) *J Mar Biol Assoc UK* 60:205–214.
7. Lichtenegger HC, Schoberl T, Bartl MH, Waite JH, Stucky GD (2002) *Science* 298:389–392.
8. Moses DN, Harreld JH, Stucky GD, Waite JH (2006) *J Biol Chem* 281:34826–34832.
9. Moses DN, Mattoni MA, Slack NL, Waite JH, Zok FW (2006) *Acta Biomater* 2:521–530.
10. Schofield RM, Nesson MH (2003) *Science* 301:1049.
11. Zahl DB, Schmauder S, McMeeking RM (1994) *Acta Metal Mater* 42:2983–2997.
12. Sole BM, Ball A (1996) *Tribol Int* 29:457–465.
13. Kukureka SN, Hooke CJ, Rao M, Liao P, Chen YK (1999) *Tribol Int* 32:107–116.
14. Cenna AA, Doyle J, Page NW, Beehag A, Dastoor P (2000) *Wear* 240:207–214.
15. Cirino M, Pipes RB, Friedrich K (1987) *J Mater Sci* 22:2481–2492.
16. Ashby MF (2005) in *Materials Selection in Mechanical Design* (Elsevier Butterworth–Heinemann, Burlington, MA), 3rd Ed, pp 283–316.
17. Broomell CC, Mattoni MA, Zok FW, Waite JH (2006) *J Exp Biol* 209:3219–3225.
18. Oliver WC, Pharr GM (1992) *J Mater Res* 7:1564–1583.